The role of healed N-vacancy defective BC_2N sheet and nanotube by NO molecule in oxidation of NO and CO gas molecules

The role of healed N-vacancy defective BC_2N sheet and nanotube by NO molecule in oxidation of NO and CO gas molecules

Parisa Nematollahi , Mehdi D. Esrafili , Erik C. Neyts

PII: S0039-6028(17)30926-3
DOI: 10.1016/j.susc.2018.03.002
Reference: SUSC 21205

To appear in: *Surface Science*

Received date: 10 December 2017
Revised date: 18 February 2018
Accepted date: 3 March 2018

Please cite this article as: Parisa Nematollahi , Mehdi D. Esrafili , Erik C. Neyts , The role of healed N-vacancy defective BC_2N sheet and nanotube by NO molecule in oxidation of NO and CO gas molecules, *Surface Science* (2018), doi: 10.1016/j.susc.2018.03.002

Highlights

- The healing of N-vacancy boron carbonitride nanosheet (NV-BC_2NNS) and nanotube (NV-BC_2NNT) by NO molecule are obtained with very low barrier energies.
- It should be noted that the obtained energy barriers of both healing and oxidizing processes are significantly lower than those of graphene, carbon nanotubes or boron nitride nanostructures.
- At the end of the oxidation process, the pure BC_2NNS or BC_2NNT is obtained without any additional defects.
- This study could be very helpful in both purifying the defective BC_2NNS and BC_2NNT while in the same effort removing toxic NO and CO gases.

The role of healed N-vacancy defective BC_2N sheet and nanotube by NO molecule in oxidation of NO and CO gas molecules

Parisa Nematollahi[1,*], Mehdi D. Esrafili[2,] and Erik C. Neyts[1]

[1]Research Group PLASMANT, Department of Chemistry, University of Antwerp, Universiteitsplein 1, 2610 Wilrijk-Antwerp, Belgium

[2] Laboratory of Theoretical Chemistry, Department of Chemistry, University of Maragheh, Maragheh, Iran

* Corresponding author. **Phone:** (+32)32652346. **E-mail**: Parisa.Nematollahi@uantwerpen.be

Abstract

In this study, the healing of N-vacancy boron carbonitride nanosheet (NV-BC_2NNS) and nanotube (NV-BC_2NNT) by NO molecule is studied by means of density functional theory calculations. Two different N-vacancies are considered in each of these structures in which the vacancy site is surrounded by either three B-atoms (NB) or by two B- and one C-atom (NBC). By means of the healed BC_2NNS and BC_2NNT as a support, the removal of two toxic gas molecules (NO and CO) are applicable. It should be noted that the obtained energy barriers of both healing and oxidizing processes are significantly lower than those of graphene, carbon nanotubes or boron nitride nanostructures. Also, at the end of the oxidation process, the pure BC_2NNS or BC_2NNT is obtained without any additional defects. Therefore, by using this method, we can considerably purify the defective BC_2NNS/BC_2NNT. Moreover, according to the thermochemistry calculations we can further confirm that the healing process of the NV-BC_2NNS and NV-BC_2NNT by NO are feasible at room temperature. So, we can claim that this study could be very helpful in both purifying the defective BC_2NNS/BC_2NNT while in the same effort removing toxic NO and CO gases.

Keywords: Healing, Boron carbonitride nanotube; BC_2NNS; BC_2NNT; Boron carbonitride nanosheet; CO oxidation; NO oxidation.

Introduction

Carbon nanotubes (CNTs) continue to attract scientific interest thanks to their unique properties, reactivity and potential applications in various areas, such as biosensors, molecular devices, and medicinal chemistry [1-3]. In particular the tunable electronic properties of CNTs have led to a significant number of studies investigating their application in nanoelectronic devices [4-7]. Contrary to CNTs whose electronic properties are strongly dependent on their radii and chiralities [8, 9], boron nitride nanotubes (BNNTs) in contrast are semiconductors characterized by a wide band-gap of about 5.5 eV, almost independent of their diameter, chirality and morphology [9-12].

Motivated by these differences, ternary boron carbonitride materials (BCN) in different forms such as cubic, layered and tubular shapes have also attracted increasing scientific interest due to their unique electronic properties and are naturally considered as ideal candidates for various applications in nanotechnology [13-17]. These ternary B–C–N materials are good semiconductors whose properties can be controlled by suitable changes in their stoichiometry [18-20]. Moreover, they have high surface area and exhibit remarkable adsorption properties [21, 22]. It is already acknowledged that, similar to graphite and hexagonal boron nitride (h-BN), hexagonal boron carbonitride ($B_xC_yN_z$) can form nanostructures, such as thin films [23, 24], composite sheets, nanofibers and nanotubes [25-27]. In a theoretical study performed by Kan et al. [28] on BCN nanoribons, it was proposed that these nanostructures can have semi-metallic properties. In homogeneously structured $B_xC_yN_z$ compounds in which carbon atoms of graphite are partially substituted by boron and nitrogen atoms, the electronic behavior of pure C and BN nanomaterials are appropriate for miniaturization of electronic devices, lightweight electrical conductors, transistors, light emission diodes, and lasers [29, 30].

Among the various ternary BCN systems, some of $C_x(BN)_y$ nanotubes and nanosheets such as BC_xN ($1 < x < 5$) [26, 31, 32], have been synthesized experimentally. It should be mentioned that the band gaps and other electronic properties of these new synthesized compounds are intermediate between those of pure carbon and BN [26, 33]. Hexagonal BC_2N is believed to be the most stable form of the ternary layers [34]. BC_2N thin films have been synthesized by means of chemical vapor deposition with BCl_3 and CH_3CN as the starting materials and the atomic arrangement and electronic structure of the monolayer structures have been studied extensively [35, 36]. It is found that the stability and electronic properties of BC_2N nanosheets (BC_2NNSs) are intermediate between those of semi-metallic graphite and insulating BN sheets. Graphene-like BC_2NNS is a semiconductor with an indirect band gap [37, 38] and similar in structure to graphene [39]. This has attracted scientific interest for possible future applications. For instance, in a theoretical study, Guo et al. [40] investigated the hydrogen storage properties of BC_2NNSs. Hydrogen adsorption energies of up to 0.11 eV were found, which was found to be slightly dependent on the adsorption site. It is noteworthy that although the binding energy of H_2 molecules on BC_2N materials is slightly higher than that on carbon nanomaterials, it is still lower than the desired adsorption energy of 0.2-0.4 eV [41, 42]. Moreover, metal decorated monolayer BC_2N was demonstrated as a high-capacity hydrogen storage medium by Wang et al. [43]. In particular, Li and Ca decorated BC_2N were systematically investigated as metal decorated BC_2N and these materials were found to be feasible for hydrogen storage without metal clustering.

BCN nanotubes have been synthesized by various methods such as electrical arc discharge [44, 45], pyrolysis [27], laser ablation [46] and more recently by laser vaporization [30]. These studies induced a large

number of theoretical investigations [47-49]. According to the studies of Miyamoto et al. [50], BCN nanotubes can be grown in three stable structures, known as type-I, type-II and type-III from which type-II should be the most stable one. Their calculations also indicated that the type-II BC_2N nanotube (BC_2NNT) has a semiconductor behavior with a band gap of about 1.6 eV. Similar to BCN nanosheets, it is expected that BC_2NNTs have electronic properties between BNNTs as a semiconductor material and CNTs whose properties depend on the tube's chirality and diameter [51]. BC_2NNTs were first synthesized by Weng-Sieh et al. [52] in 1995 by means of an arc discharge. Subsequently, other studies have been carried out to investigate e.g. the optical and elastic properties of single-walled BC_2NNTs [53, 54]. For example, Pan et al. [55] studied the electronic properties of BC_2NNTs theoretically. They found that the strain energy of BC_2NNTs shows a direct relationship with the diameter of the tube, but independent of the chirality of the tube. Moreover, the adsorption of atomic and molecular hydrogen on BC_2NNTs depends on the ionic nature of the tube surface, which may be employed in energy storage applications or molecular sensors. Wang et al. [56] investigated the structure, stability and electronic properties of ultra-thin BC_2NNTs. They indicated that the stability of BC_2NNTs is sensitive to both the number of B-N bonds and the relative ordering of the CNT and BNNT segments. All (2,2) BC_2NNTs were found to be semiconducting with tunable energy gap, whereas (4,0) BC_2NNTs can be either conducting or semiconducting depending on the configuration of the CNT and BNNT segments. Also, Guo et al. [57] studied the structural and electronic properties of armchair $C_x(BN)_y$ nanotubes, showing that such tubes have similar stabilities.

It is known that doping is an efficient approach to enhance the optical, chemical, electronic, and magnetic properties of materials such as graphene [58-60], CNTs [61, 62], BNNSs [63, 64] or BNNTs [65, 66]. This can in turn be used in gas storage, catalysts and sensing platforms. There are various investigations on decorated and doped BC_2N nanostructures [43, 67, 68]. For example Qiu et al. [69] studied the effects of Ca decoration of BC_2NNS on hydrogen storage. They found that Ca decorated BC_2NS have strong donation and back-donation of Ca with the sheets, which is responsible for enhanced binding, thus eliminating the clustering problem. In another study, Rupp et al. [70] studied the equilibrium geometry, energetic stability, and electronic properties of substitutional silicon impurities in the zigzag (5,0) and armchair (3,3) BC_2NNTs based on spin polarized density functional theory. They indicated that the Si impurities in BC_2NNTs have lower formation energy compared to Si in carbon and boron nitride nanotubes.

In the present work, we employ density functional theory (DFT) calculations to investigate the healing of N-vacancy BC_2NNS (NV-BC_2NNS) and armchair (4,4) BC_2NNT (NV-BC_2NNT) by means of NO molecule. Moreover, the removal of extra atomic O from the healed BC_2NNS and BC_2NNT by another NO or CO molecule is also investigated in detail. To the best of our knowledge, there are no previous reports on healing single vacancies in defective BC_2NNS and BC_2NNT by using NO, which is the focus of this paper. These results have practical implications for the development of novel BC_2N based nanodevices acting as gas sensor or metal-free catalysts.

Method

All calculations were performed with DFT as implemented in the Gaussian 09 package [71]. Full geometry optimization of all structures are performed at the M06-2X/6-31G* level of theory. The M06-2X density functional

is a global hybrid meta-GGA functional, with 54% HF exchange, which is widely used for studying both covalent and non-covalent interactions. In order to recognize that the optimized complexes correspond to a true local minimum or not, all the relative frequency calculations were performed at the same level of theory. We selected a BC_2NNS consisting of 44 carbon, 11 boron and 11 nitrogen atoms and the armchair (4,4) BC_2NNT containing 44 carbon, 22 boron and 22 nitrogen atoms. To avoid the unsaturated boundary effect, hydrogen atoms are added to both ends of BC_2NNT and to the edges of the BC_2NNS. The adsorption energy (E_{ads}) of the NO molecule over the NV-BC_2N nanostructures is evaluated as follows:

$$E_{ads}(NO) = E_{NO\text{-}sub} - E_{sub} - E_{NO} \quad (1)$$

where $E_{NO\text{-}sub}$, E_{Sub} and E_{NO} are the total energies of the adsorbed NO molecule over NV-BC_2NNS or NV-BC_2NNT, the pure BC_2NNS or BC_2NNT, and the NO molecule, respectively. In addition, all transition state structures were characterized by both a frequency analysis and intrinsic reaction coordinate (IRC) calculations.

Results and dissections

Geometry of NV-BC_2NNS

The partial structure of the optimized pure BC_2NNS, with three types of bonds, namely N-B, N-C and B-C, with corresponding lengths of 1.44 Å, 1.40 Å and 1.55 Å, respectively, is shown in Figure 1 (configuration **A**). In this configuration, two different kinds of N-vacancies can be considered, involving the hollow center between three B-atoms (NB) (configuration **B**) and between two B-atoms and one C-atom (NBC) (configuration **C**). In configuration **B**, a 12-membered ring is produced by the removal of one N atom. In this case, the B1–B2, B2–B3 and B1–B3 bond distances are modified, i.e., from 2.50, 2.52 and 2.50 Å in configuration **B** to 2.44, 2.35 and 2.51 Å in configuration **A**, respectively. The average bond length of the three boron atoms surrounding the vacancy increased from 1.44 Å in pure BC_2NNS to 2.43 Å in configuration **B**.

As is apparent from Figure 1, in configuration **C**, the three nearest atoms to the vacancy site are two B-atoms and one C-atom. The B1-C1, C1-B3 and B1-B3 bond lengths are modified from 2.25, 2.25 and 2.59 Å in pure BC_2NNS to 2.47, 2.46 and 2.50 Å in configuration **C**. Also, according to previous studies, the average distance between the B atoms at the vacancy site in NV-BC_2NNS (≈ 2.43 Å) is longer than that in the NV-BN nanosheets (≈ 2.33 Å) [72].

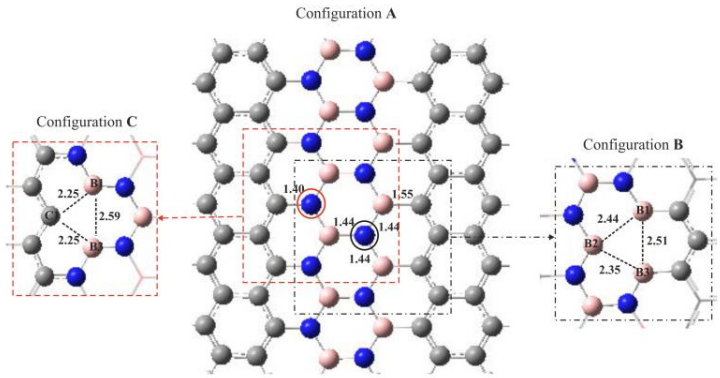

Figure 1. Optimized structures of BC_2NNS (configuration **A**) and two different NV-BC_2NNSs (configurations **B** (NB-vacancy) and **C** (NBC-vacancy)). All distances are in Å.

Healing of NV-BC_2NNS by NO

In the healing process of configurations **B** and **C** by the NO molecule, firstly, the NO molecule either physically or chemically adsorbs at the vacancy site, and then fills the vacancy. The formed N-doped BC_2NNS has an extra atomic oxygen (O_{ads}) (see Figure 2a) which by introducing the second molecule (NO or CO) to the system, can be eliminated from the surface. The corresponding structures of the healed NO molecule on configurations **B** and **C** along with their minimum energy pathway (MEP) and optimized structures for the initial state (IS), the transition state (TS) and the final state (FS) are depicted in Figure 2. Additionally, the relevant adsorption energy (E_{ads}), activation energy (E_{act}) and thermodynamic parameters for each reaction pathway such as change of Gibbs free energy (ΔG_{298}), reaction energy (ΔE), and the reaction enthalpy (ΔH_{298}) are given in Table 1.

In configuration **B**, when the NO molecule adsorbs on the boron atom of the vacancy site N-B = 2.84 Å with E_{ads} = -7.45 eV, IS-1 is formed (see Figure 2a). In TS-1, the NO molecule approaches the other B atoms of the vacancy site, causing a reduction in the N-B bond length from 2.84 Å in IS-1 to 1.69 Å in TS-1. In the next step (FS-1), the NO molecule is doped into the N-vacancy site. In this structure, the N atom binds with three B-atoms while the O atom makes a three-membered ring (3MR) connecting to the dangling bonds of B-atoms around the vacancy site. The obtained complex is termed **D** in the further discussion. Furthermore, it can be concluded from Table 1 that the energy barrier of vacancy healing in configuration **B** is very low, E_{act} = 0.10 eV, and it is a strongly exothermic process with ΔH_{298} = -5.23 eV. Also, this reaction proceeds spontaneously at room temperature (ΔG_{298} = -4.96 eV).

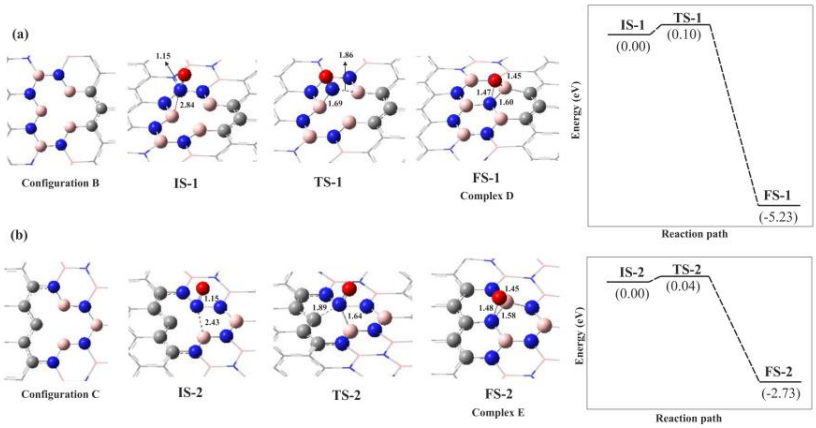

Figure 2. The optimized geometry and energy profile of the N-vacancy BC_2NNS recombination process by NO molecule adsorption onto configurations **B** (a) and **C** (b). All energy values and distances are in eV and Å, respectively. Color code for each optimized structure: Blue ball: N; red bull: O, pink ball: B and gray ball: C.

By introducing the NO molecule to configuration **C**, the vertically oriented NO molecule is positioned above the B atom of the vacancy with a bond length B-N = 2.43 Å (see Figure 2b). The adsorption energy E_{ads} = -7.35 eV, which shows the strong binding of the NO molecule to the vacancy site. In TS-2, the NO molecule approaches to C atom of the vacancy site, with bond length N–C = 1.89 Å, while the B-N bond length is reduced to 1.64 Å. The activation energy of this step is almost negligible ($E_{act} \approx 0.04$ eV). In the next step, the NO molecule is doped into the vacancy site and forms FS-2, which we indicate as complex **E** in the further discussion. Analogous with complex **D**,

a 3MR is formed with three B–O, N–O and B–N bond lengths of 1.45, 1.48 and 1.58 Å, respectively. It can be seen from Table 1 that the reaction pathway IS-2 → FS-2 is an exothermic process with ΔH_{298} = -2.72 eV. Also, this reaction is spontaneous at room temperature (ΔG_{298} = -2.07 eV). According to our results, the healing energy barriers of configurations **B** and **C** are lower than those in previous studies. For instance, Feng et al. [73] reported the energy barrier of 0.25 eV for healing of N vacancy by NO_2 molecule.

Table 1. Calculated adsorption energy (E_{ads}) of adsorbed NO molecule over NV-BC_2NNS, along with their corresponding activation energy (E_{act}), reaction energy (ΔE), change of Gibbs free energy (ΔG_{298}) and change of enthalpy (ΔH_{298}) for the healing process of NV-BC_2NNS by NO molecule

Pathways	E_{ads} (eV)	E_{act} (eV)	ΔE (eV)	ΔG_{298} (eV)	ΔH_{298} (eV)
IS-1 → FS-1	-7.45	0.10	-5.23	-4.96	-5.23
IS-2 → FS-2	-7.35	0.04	-2.73	-2.07	-2.72

Oxygen removal of the healed BC_2NNS by NO

It was previously found that the adsorbed atomic oxygen atom over CNTs or SiCNTs can be eliminated from the surface by introducing a second CO [66, 74], N_2O [75, 76] or second NO molecule [77]. So, here, the removal of extra atomic O by introducing the second NO molecule to the system is investigated in detail. In order to better understand this process, all the IS, TS and FS configurations along with their MEP diagrams, are depicted in Figure 3. In addition, the corresponding activation energy and thermodynamic properties (ΔG_{298}, ΔH_{298}, ΔE) are listed in Table 2. By introducing the NO molecule to complex **D**, IS-3 is formed in which the NO molecule is placed in a tilted position above the 3MR with bond length N-O_{ads} = 2.94 Å (see Figure 3a). Then, by passing via TS-3 with energy barrier of 0.8 eV the NO_2 molecule can be formed. In this structure, the NO molecule approaches to O_{ads}, with bond length O–N = 1.89 Å. In FS-3, the physically adsorbed NO_2 molecule over the BC_2NNS with bond length B-O = 3.05 Å is produced in a parallel position to the surface. Finally, the NO_2 molecule can easily desorb from the BC_2NNS due to the small adsorption energy E_{ads} = -0.25 eV. In addition, according to Table 2, the formation of NO_2 molecule is exothermic with ΔH_{298} = -1.47 eV and is thermodynamically favorable at room temperature (ΔG_{298} = -1.50 eV).

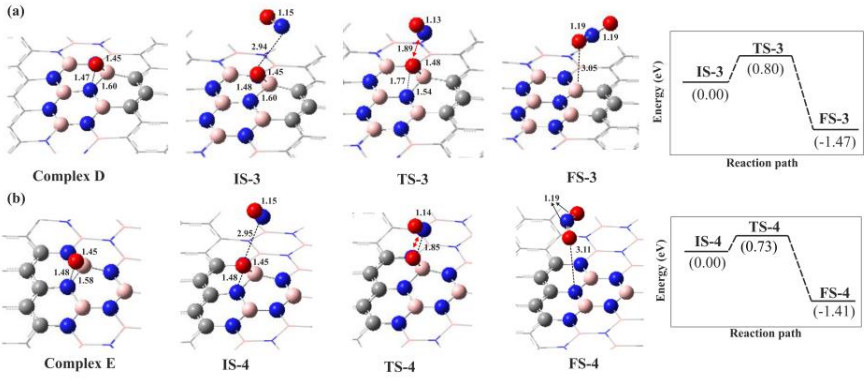

Figure 3. The optimized geometry and reaction profiles of NO oxidation reaction over the healed BC_2NNS surface by NO molecule. All distances are in Å

Similarly, when the NO molecule is added to complex **E**, the same reaction occurs: in IS-4, the NO molecule approaches the attached O atom, with bond length N-O_{ads} = 2.95 Å (see Figure 3b). TS-4 is characterized by an activation energy E_{act} = 0.73 eV, indicating that the B-O and N-O bonds can easily break, which facilitates the interaction of the O_{ads} with the second NO molecule. In this configuration, the N atom of the NO molecule approaches the O_{ads} in order to form the NO_2 molecule. The formed NO_2 molecule lies almost parallel to the surface, at a distance of N-O = 3.11 Å. In FS-4, the N=O bond length of the physisorbed NO_2 molecule increases from 1.15 Å in IS-4 to 1.19 Å in the NO_2 gas form. This gas molecule can then be easily released from the BC_2NNS surface due to its low adsorption energy, E_{ads} = -0.30 eV. Also, upon desorption of NO_2, the pure defect-free BC_2NNS is obtained. The reaction pathway IS-4 → FS-4 is also exothermic, with ΔH_{298} = -1.41 eV, and is thermodynamically spontaneous at ambient conditions (ΔG_{298} = -1.51 eV). The obtained energy barrier values are lower than those reported in Wang et al. [78] investigation.

Table 2. Calculated activation energy (E_{act}), reaction energy (ΔE), change of Gibbs free energy (ΔG_{298}) and change of enthalpy (ΔH_{298}) for the NO oxidation over the healed BC_2NNS by NO molecule

Pathways	E_{act} (eV)	ΔE (eV)	ΔG_{298} (eV)	ΔH_{298} (eV)
IS-3 → FS-3	0.80	-1.47	-1.50	-1.47
IS-4 → FS-4	0.73	-1.41	-1.51	-1.41

Geometry of NV-BC_2NNT

We also studied the healing of the N-vacancy by an NO molecule over the armchair (4,4) BC_2NNT. In order to achieve this, a tubular armchair (4,4) BC_2NNT is used as shown in Figure 4 (configuration **F**). There are three different bonds: C–N, C–B and B–N with bond lengths of 1.38, 153 and 1.45 Å, respectively. Analogous with BC_2NNS, removing one N atom from two different positions in the middle of BC_2NNT, two ideal single N-vacancy defects are produced: NB and NBC. These two possible defect sites for the N-vacancy BC_2NNT are depicted as configurations **G** and **H** (see Figure 4).

In complex **G**, the N-vacancy defective BC_2NNT is produced by removing one N atom which is surrounded by three closest B atoms (B1, B2 and B3): NB. Upon the removal of the N atom, the two B atoms near the vacancy site (B2 and B3) move so close to each other that their binding distance (≈ 1.77 Å) becomes smaller than that in pristine BC_2NNT (2.49 Å), thereby forming a 5-membered ring (5MR). In this configuration, the binding distances of the B atoms (B1–B3 and B2–B3) in the remaining 9-membered ring decrease from 2.38 Å in pristine BC_2NNT to 2.02 and 2.31 Å in the defected tube, respectively (see Figure 4). These data are also close to other studies in related BN structures [79]. For instance, Xiao et al. [77] reported theoretically that the B2-B3 bond length in the N vacancy BNNT is about 1.78 Å and these two-coordinated B atoms in the defect protrudes from the circumference of the tube.

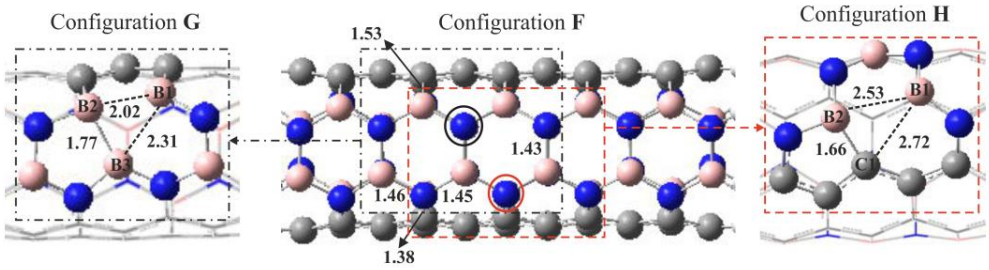

Figure 4. Optimized structures of BC_2NNT (configuration **F**) and two different NV-BC_2NNTs (configurations **G** (NB-vacancy) and **H** (NBC-vacancy)). All distances are in Å

Configuration **H** is the same structural configuration as complex **G**, but in this case the vacancy is surrounded by two B-atoms (B1, B3) and one C-atom (C1): NBC. Analogous to configuration **G**, the two nearest B1 and C1 atoms at the vacancy site approach each other and form a 5MR upon removal of the N atom. Again the two B2 and C1 atoms bind together with a bond distance B2–C1 = 1.66 Å, which is smaller than that in complex G (1.77 Å) and in pristine BC_2NNT (2.42 Å). Also, the other binding distances of B1–B2 and B1–C1 in the remaining 9-membered ring increase from 2.49 and 2.42 Å in pure BC_2NNT to 2.53 and 2.72 Å in the defected tube, respectively (see Figure 4).

Healing of NV-BC_2NNT by NO

In the case of BC_2NNT, the healing process of NV-BC_2NNT by an NO molecule proceeds similar to NV-BC_2NNS via two main steps: (1) the physical or chemical adsorption of the NO molecule at the vacancy site and (2) removing the O_{ads} by another NO molecule. The optimized structures of the NO molecule over configurations **G** and **H** along with their MEP diagram and their corresponding stationary points (IS, TS and FS) are shown in Figure 5. Moreover, the geometric and thermodynamic properties of these reaction pathways are listed in Table 3. By adding a NO molecule to the complex **G**, IS-5 is obtained. In this structure, the NO molecule is chemically attached to the B atom of the vacancy site. As a result, the B atom protrudes somewhat out of the tube surface with bond lengths B–O = 1.52 Å and N=O = 1.12 Å. The distance between the N atom and the other two B atoms of the vacancy is 3.28 and 2.60 Å, respectively. In addition, the high adsorption energy E_{ads} = -8.17 eV indicates that there is a great tendency for NO molecule to react with the NB vacancy site of BC_2NNT. In TS-5 the NO molecule approaches both B atoms of the vacancy site via its N and O atoms. In this structure, the N-B and O-B bond lengths are 2.55 and 2.10 Å, respectively, which causes the elongation and also activation of the N-O bond from 1.22 Å in IS-5 to 1.25 Å in this state. By overcoming a low energy barrier of 0.65 eV, the NO molecule heals the N-vacancy site of BC_2NNT, yielding the FS-5 configuration in which the NO molecule forms a three-membered ring with B-O, N-O and B-N bond lengths of 1.40, 1.44 and 2.08 Å, respectively. It can be concluded from the high values for the thermodynamic properties that the healing of the N-vacancy in BC_2NNT by NO is exothermic (ΔH_{298} = -5.95 eV) and occurs at room temperature (ΔG_{298} = -5.82 eV).

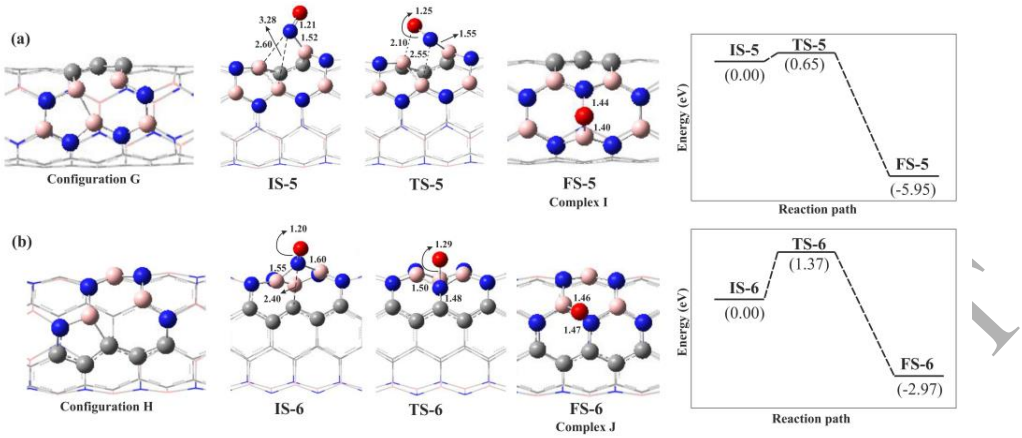

Figure 5. The optimized geometry and energy profile of the N-vacancy BC_2NNT recombination process by NO molecule adsorption onto configurations **G** (a) and **H** (b) along with their relative energy profile. All energy values and distances are in eV and Å, respectively. Color code for each optimized structure: Blue ball: N; red bull: O, pink ball: B and gray ball: C.

As shown in Figure 5b, upon introducing the second NO molecule to configuration **H**, IS-6 is formed where the NO molecule is positioned right in the middle of the vacancy site and binds with two B-atoms with average bond lengths of 1.57 Å and an adsorption energy E_{ads} = -5.75 eV, while it is somewhat far from the C atom, N-C = 2.40 Å. In TS-6, the N atom approaches the C atom to make a chemical bond. In FS-6, a stable three-membered ring is formed in which the O atom is placed between two B-atoms and a N-atom with B-O, N-O and B-N bond lengths of 1.46, 1.47 and 1.57 Å, respectively (see Figure 5b). In this structure, the formed N-C bond is 1.48 Å and the N-O bond is elongated from 1.20 Å in IS-6 to 1.29 Å. +The activation energy of this path IS-6 → FS-6, is calculated as E_{act} = 1.37 eV, which is higher than that in IS-5 → FS-5. Again, the reaction is exothermic and spontaneous at room temperature (see Table 3). The healing process of N-vacancy BC_2NNT by No molecule has lower energy barrier than that in BNNT studied by Xiao et al. [77]. Experimental results show that the synthesized BNNTs have nanoscaled diameters, in the range of several to several tens of nanometers (0.95 nanometers in (12, 0) BNNT). Therefore, the healing energy barrier of the N-vacancy in BNNT by NO will be within the range from 0.41 to 0.54 eV in the real cases. This is almost near to the obtained theoretical value of the healing of N-vacancy BC_2NNT by NO molecule (see Figure 5, configuration G).

Table 3. Calculated adsorption energy (E_{ads}) of adsorbed NO molecule over NV-BC_2NNT, along with their corresponding activation energy (E_{act}), reaction energy (ΔE), change of Gibbs free energy (ΔG_{298}) and change of enthalpy (ΔH_{298}) for the healing of process of NV-BC_2NNT by NO molecule

Pathways	E_{ads} (eV)	E_{act} (eV)	ΔE (eV)	ΔG_{298} (eV)	ΔH_{298} (eV)
IS-5 → FS-5	-8.17	0.65	-5.95	-5.82	-5.95
IS-6 → FS-6	-5.75	1.37	-2.65	-2.56	-2.65

Oxygen removal of the healed BC_2NNT by NO

Finally, we studied the removal of O_{ads} from BC_2NNT using the second NO molecule. The geometries of the related IS, TS and FS configurations are shown in Figure 6. Also, the related activation energy and thermodynamic properties are listed in Table 4. The oxidation reaction starts by introducing the NO molecule to

complex **I,** named IS-7. After relaxation, the NO molecule is placed horizontally on top of the tube surface with N-O_{ads} = 2.89 Å. Then, it approaches the O_{ads} in order to make a chemical bond with it (TS-7). In this state, the N-O_{ads} bond length decreases to 1.83 Å while the N=O bond length decreases from 1.15 Å in IS-7 to 1.13 Å. The energy barrier of this step is 1.61 eV which eventually results in the formation of an NO_2 molecule in FS-7. In this stage, the NO_2 molecule is physically adsorbed over the BC_2NNT (O-B = 2.85 Å), and can easily desorbs from the surface (E_{ads} = -0.18 eV). The formed NO_2 molecule has bond lengths for N=O = 1.19 Å which is the same as that in the gas phase. In contrast to all previous pathways, this reaction IS-7 → FS-7 is endothermic with the reaction enthalpy of ΔH_{298} = 0.64 eV (Table 4) and the positive value of ΔG_{298} indicates that it is not favorable thermodynamically.

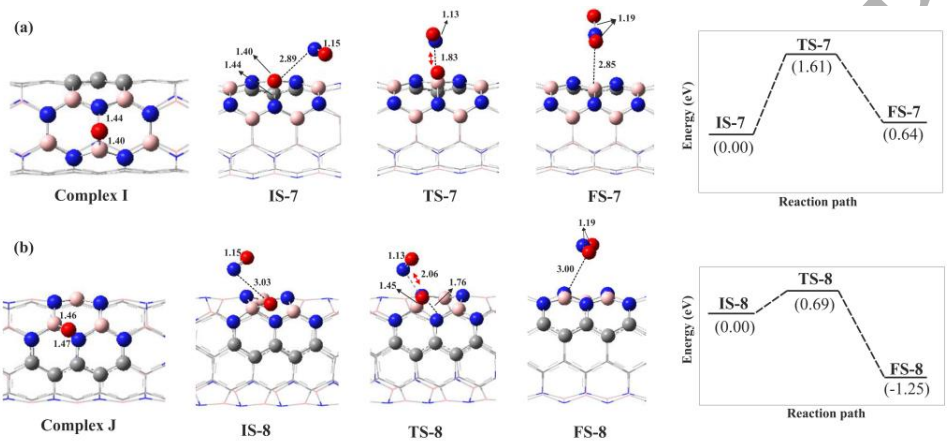

Figure 6. The optimized geometry and reaction profiles of NO oxidation reaction over the healed BC_2NNT surface by NO molecule. All distances are in Å

Next, we investigate the same reaction starting with complex **J.** Introduction of the second NO results in IS-8. After optimization, the NO molecule is positioned on top of the O_{ads}, with distance N-O_{ads} = 3.03 Å (see Figure 6b). When the NO molecule approaches the O_{ads} to a distance of 2.06 Å in TS-8, the NO_2 molecule can produce. The activation energy of this step is 0.69 eV which is in close agreement with Liu et al. [72] study. Finally, the NO_2 molecule is formed in FS-8 and released from the BC_2NNT surface because of the low adsorption energy, E_{ads} = -0.29 eV. According to obtained results listed in Table 4, the pathway is exothermic and the reaction proceeds spontaneously at room temperature (ΔG_{298} = -1.28 eV). The obtained energy barriers of O-removal by NO molecule over BC_2NNT are lower than those in BNNT [77].

Table 4. Calculated activation energy (E_{act}), reaction energy (ΔE), change of Gibbs free energy (ΔG_{298}) and change of enthalpy (ΔH_{298}) for the NO oxidation over the healed BC_2NNT by NO molecule

Pathways	E_{act} (eV)	ΔE (eV)	ΔG_{298} (eV)	ΔH_{298} (eV)
IS-7 → FS-7	1.61	0.64	0.51	0.64
IS-8 → FS-8	0.69	-1.25	-1.28	-1.25

Oxygen removal of the healed BC_2NNS and BC_2NNT by CO

We also studied the removal of the adsorbed atomic oxygen over the BC_2NNS and BC_2NNT by introducing a CO molecule as another toxic gas present in the air in order to form the CO_2 molecule. All the geometric structures of IS, TS and FS along with their MEP diagram, are depicted in Figures S1 and S2 (Supporting Information). Additionally, the corresponding energy barrier and thermodynamic parameters (ΔG_{298}, ΔH_{298}, ΔE) are listed in Tables S1 and S2 (Supporting Information). All the detailed steps are the same as those found for NO oxidation. Starting with configuration **D**, the CO molecule is positioned over the O_{ads} with C-O_{ads} = 3.02 Å yielding IS-9. As is apparent from Figure S1, in FS-9 the CO_2 gas molecule can be released from the surface due to the small adsorption energy, E_{ads} = -0.23 eV. The E_{act} of pathway IS-9 → FS-9 is 1.03 eV and it is an exothermic reaction with ΔH_{298} = -3.98 eV. Moreover, it is thermodynamically favorable at ambient conditions (see Table S1).

Addition of CO molecule to configuration **E** forms IS-10 in which the CO molecule is located at a distance of 2.52 Å from O_{ads} (see Figure S1b). In approaching the adsorbed O atom in order to produce the CO_2 gas molecule, only a small activation barrier E_{act} = 0.07 eV is encountered .Overall, the reaction pathway IS-10 → FS-10 is exothermic with ΔH_{298} = -4.38 eV and is thermodynamically feasible (ΔG_{298} = -4.27 eV) at room temperature. Similar to NO_2, the CO_2 molecule can easily desorb from the BC_2NNS surface (E_{ads}= -0.25 eV).

For studying the O removal by CO on BC_2NNT surface, we start with configurations **I** and **J** (Figure S2a). It is noteworthy that because of the strong interaction between the O atom and the BC_2NNT, there are high energy barriers for the direct removal of atomic O in both configurations. Introducing a CO molecule to configuration **I** lead to the formation of IS-11. Passing via TS-11 with an energy barrier of 1.85 eV results in FS-11 in which the CO_2 molecule is formed. In this stage, the CO_2 molecule is parallel to the surface, and is physically adsorbed over the BC_2NNT (E_{ads} = -0.16 eV). The reaction pathway IS-11 → FS-11 is exothermic with ΔH_{298} = -1.99 eV (Table S2).

When the CO molecule is introduced to configuration **J** at a distance of 3.00 Å from O_{ads}, IS-12 is formed (Figure S2b). The CO_2 molecule is then produced passing via TS-12 with a significant energy barrier of 2.74 eV. In FS-12, the CO_2 molecule with a weak adsorption energy E_{ads} = -0.29 eV is produced and desorbs from the BC_2NNT surface. This reaction is also exothermic and favorable at room temperature (ΔH_{298} = -2.05 eV and ΔG_{298} = -1.99 eV).

According to experimental investigations, single X-vacancy nanostructures can be easily introduced through electron or ion-irradiation [80, 81]. They contain unsaturated atoms and therefore, they are highly reactive. Accordingly, healing of these single X-vacancy nanostructures by certain foreign molecules, especially gas molecules containing an X atom (here the NO molecule) or atoms with a similar size and reactivity as X, are favored, typically making the reaction pathway exothermic and spontaneous at room temperature. In this study, the NBC vacancy in both BC_2NNS and BC_2NNT shows lower activation energy toward the NO healing. Also, removal of the adsorbed oxygen atom by introducing the second NO or CO molecule in NBC vacancy proceeds via lower activation energy than that in NB vacancy. Generally, it is found that reactions with a barrier of less than 0.5 eV are expected to occur at room temperature; correspondingly, we here find that the energy barrier for O-removal by NO molecule is low on NBC vacancy BC_2NNS and BC_2NNT and these reactions can easily occur at room temperature.

Conclusion

We have investigated the healing of the NV-BC_2NNS and NV-BC_2NNT by using NO molecule using detailed DFT calculations. Two different vacancies are chosen for each nanostructure: NB and NBC. We found that the defect formation energy in NV-BNC_2NNT is smaller than NV-BC_2NNS. This can be due to the covalent B-B interaction which leads to the formation of a 5MR in the nanotube surface, which favors the formation of a N-vacancy in this system. For both NV-nanostructures, the defect site is the most active area for the healing process by NO molecule. Thus, addition of a second NO molecule to the N-vacancy site can be expected to be a favorable reaction and can be viewed as the first step of the healing of NV-BC_2NNS and NV-BC_2NNT surfaces. The adsorption energy of NO molecule over NB and NBC vacancies of BC_2NNS is calculated as -7.45 eV and -7.35 eV while it was -8.17 eV and -5.75 eV in BC_2NNT, respectively. This indicates the strong interaction between NO and NV-BC_2N nanostructures. But, in comparison to NV-BC_2NNT, the healing of both N-vacancies (NB and NBC) of BC_2NNS proceeds via a lower activation energy.

Subsequently, the introduction of a second NO or CO molecule can remove the O_{ads} on the BC_2NNS and BC_2NNT. In O-removal by a second NO molecule, the NBC vacancy of BC_2NNS and BC_2NNT shows moderate activation energies (0.73 eV and 0.69 eV), which are lower than those of NB vacancies. In the O-removal by a CO molecule, the NBC vacancy of BC_2NNS shows lower barrier energy (0.07 eV) than that of NBC vacancy BC_2NNT (2.74 eV). Thus, we can conclude that the NO molecule could be a promising candidate to heal the N-vacancy defects in BC_2NNS and BC_2NNT. Moreover, although both NB and NBC vacancy BC_2NNS showed a better reactivity toward the removal of O_{ads} with NO and CO molecule, NBC vacancy BC_2NNS has lower energy barrier than NB vacancy in O-removal by a second NO molecule. According to these results we can claim that this study could be very helpful in both purifying the defective BC_2NNS/BC_2NNT while in the same effort removing toxic NO and CO gases.

Acknowledgements

The authors gratefully acknowledge support of the Research Fund of the University of Antwerp.

References

[1] T. Dinadayalane, J.S. Murray, M.C. Concha, P. Politzer, J. Leszczynski, J. Chem. Theory Comput., 6 (2010) 1351-1357.
[2] H. Chu, L. Wei, R. Cui, J. Wang, Y. Li, Coordination Chemistry Reviews, 254 (2010) 1117-1134.
[3] A. Hirsch, Angewandte Chemie International Edition, 41 (2002) 1853-1859.
[4] R. Saito, G. Dresselhaus, M.S. Dresselhaus, World Scientific, 1998.
[5] N. Hamada, S.-i. Sawada, A. Oshiyama, Phys. Rev. Lett., 68 (1992) 1579.
[6] H. Dai, Accounts of chemical research, 35 (2002) 1035-1044.
[7] M.S. Dresselhaus, P. Avouris, Introduction to carbon materials research, in: Carbon nanotubes, Springer, 2001, pp. 1-9.
[8] M. Dresselhaus, G. Dresselhaus, R. Saito, Carbon, 33 (1995) 883-891.
[9] X. Blase, A. Rubio, S. Louie, M. Cohen, EPL (Europhysics Letters), 28 (1994) 335.
[10] B. Akdim, R. Pachter, X. Duan, W.W. Adams, Phys. Rev. B, 67 (2003).
[11] N.G. Chopra, R. Luyken, K. Cherrey, V.H. Crespi, M.L. Cohen, S.G. Louie, A. Zettl, Science, 269 (1995) 966-967.
[12] D. Golberg, Y. Bando, C.C. Tang, C.Y. Zhi, Adv. Mater., 19 (2007) 2413-2432.
[13] A. Du, Y. Chen, Z. Zhu, G. Lu, S.C. Smith, J. Am. Chem. Soc., 131 (2009) 1682-1683.
[14] S. Azevedo, R. De Paiva, J. Kaschny, Journal of Physics: Condensed Matter, 18 (2006) 10871.
[15] S.Y. Kim, J. Park, H.C. Choi, J.P. Ahn, J.Q. Hou, H.S. Kang, J. Am. Chem. Soc., 129 (2007) 1705-1716.
[16] M. Matos, S. Azevedo, J. Kaschny, Solid State Communications, 149 (2009) 222-226.
[17] R.B. Kaner, J.J. Gilman, S.H. Tolbert, Science, 308 (2005) 1268-1269.
[18] E. Bengu, M.F. Genisel, O. Gulseren, R. Ovali, Thin Solid Films, 518 (2009) 1459-1464.
[19] M. Kawaguchi, T. Kawashima, T. Nakajima, Chem. Mater., 8 (1996) 1197-1201.
[20] W. Wang, X. Bai, K. Liu, Z. Xu, D. Golberg, Y. Bando, E. Wang, J. Am. Chem. Soc., 128 (2006) 6530-6531.
[21] D. Portehault, C. Giordano, C. Gervais, I. Senkovska, S. Kaskel, C. Sanchez, M. Antonietti, Adv. Funct. Mater., 20 (2010) 1827-1833.
[22] K. Raidongia, A. Nag, K. Hembram, U.V. Waghmare, R. Datta, C. Rao, Chemistry–A European Journal, 16 (2010) 149-157.
[23] D.H. Kim, E. Byon, S. Lee, J.-K. Kim, H. Ruh, Thin Solid Films, 447 (2004) 192-196.
[24] M. Lei, Q. Li, Z. Zhou, I. Bello, C. Lee, S. Lee, Thin Solid Films, 389 (2001) 194-199.
[25] X. Bai, J. Yu, S. Liu, E. Wang, Chem. Phys. Lett., 325 (2000) 485-489.
[26] L.-W. Yin, Y. Bando, D. Golberg, A. Gloter, M.-S. Li, X. Yuan, T. Sekiguchi, J. Am. Chem. Soc., 127 (2005) 16354-16355.
[27] R. Sen, B. Satishkumar, A. Govindaraj, K. Harikumar, G. Raina, J.-P. Zhang, A. Cheetham, C. Rao, Chem. Phys. Lett., 287 (1998) 671-676.
[28] E.-J. Kan, X. Wu, Z. Li, X.C. Zeng, J. Yang, J. Hou, J. Chem. Phys., 129 (2008) 084712.
[29] J. da Rocha Martins, H. Chacham, ACS Nano, 5 (2010) 385-393.
[30] S. Enouz, O. Stéphan, J.-L. Cochon, C. Colliex, A. Loiseau, Nano Lett., 7 (2007) 1856-1862.
[31] K. Raidongia, D. Jagadeesan, M. Upadhyay-Kahaly, U. Waghmare, S.K. Pati, M. Eswaramoorthy, C. Rao, J. Mater. Chem., 18 (2008) 83-90.
[32] R. Majidi, Physica E., 74 (2015) 371-376.
[33] X. Blase, H. Chacham, Electronic Properties of Boron-Nitride and Boron Carbonitride Nanotubes and Related Heterojunctions, in: BCN Nanotubes and Related Nanostructures, Springer, 2009, pp. 83-103.
[34] J. Kouvetakis, T. Sasaki, C. Shen, R. Hagiwara, M. Lerner, K. Krishnan, N. Bartlett, Synthetic metals, 34 (1989) 1-7.
[35] J.P. Nicolich, F. Hofer, G. Brey, R. Riedel, Journal of the American Ceramic Society, 84 (2001) 279-282.
[36] A.Y. Liu, R.M. Wentzcovitch, M.L. Cohen, Phys. Rev. B, 39 (1989) 1760.
[37] Y. Chen, J. Barnard, R. Palmer, M. Watanabe, T. Sasaki, Phys. Rev. Lett., 83 (1999) 2406.
[38] Z. Pan, H. Sun, C. Chen, Phys. Rev. B, 73 (2006) 193304.
[39] Z. Huang, V.H. Crespi, J.R. Chelikowsky, Phys. Rev. B, 88 (2013) 235425.
[40] J.-H. Guo, H. Zhang, Structural Chemistry, 22 (2011) 1039-1045.
[41] R.C. Lochan, M. Head-Gordon, Phys. Chem. Chem. Phys., 8 (2006) 1357-1370.
[42] S.K. Bhatia, A.L. Myers, Langmuir, 22 (2006) 1688-1700.
[43] Y.S. Wang, P.F. Yuan, M. Li, W.F. Jiang, Q. Sun, Y. Jia, Comput. Mater. Sci., 60 (2012) 181-185.

[44] O. Stephan, P. Ajayan, C. Colliex, P. Redlich, Science, 266 (1994) 1683.
[45] P. Redlich, J. Loeffler, P. Ajayan, J. Bill, F. Aldinger, M. Rühle, Chem. Phys. Lett., 260 (1996) 465-470.
[46] Y. Zhang, H. Gu, K. Suenaga, S. Iijima, Chem. Phys. Lett., 279 (1997) 264-269.
[47] X. Blase, Comput. Mater. Sci., 17 (2000) 107-114.
[48] X. Blase, J.-C. Charlier, A. De Vita, R. Car, Applied Physics A, 68 (1999) 293-300.
[49] H. Pan, Y.P. Feng, J.Y. Lin, Phys. Rev. B, 73 (2006) 035420.
[50] Y. Miyamoto, A. Rubio, M.L. Cohen, S.G. Louie, Phys. Rev. B, 50 (1994) 4976.
[51] J. Rossato, R. Baierle, W. Orellana, Phys. Rev. B, 75 (2007) 235401.
[52] Z. Weng-Sieh, K. Cherrey, N.G. Chopra, X. Blase, Y. Miyamoto, A. Rubio, M.L. Cohen, S.G. Louie, A. Zettl, R. Gronsky, Phys. Rev. B, 51 (1995) 11229.
[53] M. Terrones, D. Golberg, N. Grobert, T. Seeger, M. Reyes-Reyes, M. Mayne, R. Kamalakaran, P. Dorozhkin, Z.C. Dong, H. Terrones, Adv. Mater., 15 (2003) 1899-1903.
[54] T. Pankewitz, W. Klopper, J. Phys. Chem. C., 111 (2007) 18917-18926.
[55] H. Pan, Y.P. Feng, J. Lin, Phys. Rev. B, 74 (2006) 045409.
[56] Y. Wang, B. Zhou, X. Yao, G. Huang, J. Zhang, Q. Shao, Chem. Phys. Lett., 616 (2014) 61-66.
[57] C. Guo, W. Fan, Z. Chen, R. Zhang, Solid state communications, 137 (2006) 549-552.
[58] X.-Y. Liang, N. Ding, S.-P. Ng, C.-M.L. Wu, Appl. Surf. Sci., 411 (2017) 11-17.
[59] Y. Tong, Y. Wang, Q. Wang, Structural Chemistry, (2017).
[60] S. Li, Z. Lu, Y. Zhang, D. Ma, Z. Yang, Phys. Chem. Chem. Phys., 19 (2017) 9007-9015.
[61] M. Yoosefian, M. Zahedi, A. Mola, S. Naserian, Appl. Surf. Sci., 349 (2015) 864-869.
[62] X. Zhang, Z. Dai, Q. Chen, J. Tang, Physica Scripta, 89 (2014) 065803.
[63] Y.-j. Liu, B. Gao, D. Xu, H.-m. Wang, J.-x. Zhao, Phys. Lett. A., 378 (2014) 2989-2994.
[64] J. Zhao, Z. Chen, J. Phys. Chem. C., 119 (2015) 26348-26354.
[65] Z.-Y. Deng, J.-M. Zhang, K.-W. Xu, Appl. Surf. Sci., 347 (2015) 485-490.
[66] S. Lin, X. Ye, J. Huang, Phys. Chem. Chem. Phys., 17 (2015) 888-895.
[67] A.A. Peyghan, M. Noei, Comput. Mater. Sci., 82 (2014) 197-201.
[68] N. Song, Y. Wang, Q. Sun, Y. Jia, Appl. Surf. Sci., 263 (2012) 182-186.
[69] N.-x. Qiu, Z.-y. Tian, Y. Guo, C.-h. Zhang, Y.-p. Luo, Y. Xue, Int. J. Hydrogen Energ., 39 (2014) 9307-9320.
[70] C. Rupp, J. Rossato, R. Baierle, J. Chem. Phys., 130 (2009) 114710.
[71] M. Frisch, G. Trucks, H.B. Schlegel, G. Scuseria, M. Robb, J. Cheeseman, G. Scalmani, V. Barone, B. Mennucci, G. Petersson, Wallingford, CT, 19 (2009) 227-238.
[72] Z. Liu, Q. Xue, T. Zhang, Y. Tao, C. Ling, M. Shan, J. Phys. Chem. C., 117 (2013) 9332-9339.
[73] J.-w. Feng, Y.-J. Liu, J.-x. Zhao, J. Mol. Model., 20 (2014) 1-7.
[74] P. Nematollahi, M.D. Esrafili, New Journal of Chemistry, 40 (2016) 2775-2784.
[75] S. Wannakao, T. Nongnual, P. Khongpracha, T. Maihom, J. Limtrakul, J. Phys. Chem. C., 116 (2012) 16992-16998.
[76] S. Pornsatitworakul, S. Phikulthai, S. Namuangruk, B. Boekfa, Catalytic oxidation of CO with N2O on Fe-porphyrin catalyst, in: Science and Technology (TICST), 2015 International Conference on, IEEE, 2015, pp. 225-229.
[77] B. Xiao, X.-f. Yu, Y.-h. Ding, RSC Adv., 4 (2014) 22688-22696.
[78] B. Wang, S. Pantelides, Phys. Rev. B, 83 (2011) 245403.
[79] Y. Li, Z. Zhou, J. Zhao, Nanotechnology, 19 (2008) 015202.
[80] A. Zobelli, A. Gloter, C.P. Ewels, C. Colliex, Phys. Rev. B, 77 (2008) 045410.
[81] J. Kotakoski, A. Krasheninnikov, U. Kaiser, J. Meyer, Phys. Rev. Lett., 106 (2011) 105505.

Graphical Abstract